Supporting Information for

Reversible Medium Dependent Solid-Solid Phase Transformations in 2D Hybrid Perovskites

Cauê F. Ferreira,[a] Eduardo E. Pérez-Cordero,[a] Khalil A. Abboud,[a] and Daniel R. Talham[a*]

[a]Department of Chemistry, University of Florida, Gainesville, FL, USA

Table of Contents

S1) Thermodynamic Data for the Phase Transition of C6MnCl

Table S1. Experimental thermodynamic data of the structural phase transition for the C6MnCl hybrid perovskite dry and immersed in toluene.

$(C_6H_{13}NH_3)_2MnCl_4$	dry	in toluene
T_{trs} (K)	290.78 ± 0.50	268.38 ± 0.82
ΔH_{trs} (kJ/mol)	5.58 ± 0.12	3.40 ± 0.27
ΔS_{trs} (J/mol.K)	19.18 ± 0.40	12.65 ± 1.00

*the full DSC scans were collected from 193 to 333 K for both dry and in toluene states.

S2) Single Crystal X-ray Diffraction Structure Refinement for the LTP and HTP of C6CuCl

Low-temperature phase structure (233 K)

Raw data frames were read by the program SAINT and integrated using 3D profiling algorithms. The resulting data were reduced to produce hkl reflections and their intensities and estimated standard deviations. The data were corrected for Lorentz and polarization effects and numerical absorption corrections were applied based on indexed and measured faces.

The structure was solved and refined in SHELXTL6.1, using full-matrix least-squares refinement. The non-H atoms were refined with anisotropic thermal parameters and all of the H atoms were calculated in idealized positions and refined riding on their parent atoms. The asymmetric unit consists of two $CuCl_4^{-2}$ anions and four $C_6H_{13}NH_3^{+1}$ cations. All four alkyl chains are disordered and each one was refined in two parts with their site occupation factors adding up to unity. Each chain was also restrained by commands DFIX to maintain ideal geometries in distances and angles. Each disordered part also was restrained to maintain similar displacement parameters using the EADP command. All of the amino protons were obtained from a Difference Fourier map and refined freely. Surprisingly, all three protons on each nitrogen atom were not significantly affected by the alkyl chain disorders. The structure shows extensive H-bonding interaction between the amino protons and the chlorine atoms of the anions. In the final cycle of refinement of the low temperature phase, 9198 reflections (of which 6343 are observed with $I > 2\sigma(I)$) were used to refine 327 parameters and the resulting R_1, wR_2 and S (goodness of fit) were 5.42%, 16.39% and 1.053, respectively. The refinement was carried out by minimizing the wR_2 function using F^2 rather than F values. R_1 is calculated to provide a reference to the conventional R value but its function is not minimized.

The low-temperature phase structure could be solved with two different unit cell parameters, a large unit cell (a = 10.4935(4), b = 10.5081(4), c = 18.6574(7), α = 81.916(1), β = 79.45591), γ = 88.315(1)), and a smaller unit cell (a = 7.3171(3), b = 7.5355(3), c = 18.4840(8), α = 79.6313(7), β = 88.2145(7), γ = 90.9196(7)). However, the structure solved using the small triclinic unit cell introduces an extra element of disorder beyond of what is observed with the large unit cell. While in the large triclinic unit cell all C6 groups are lined up parallel to each other, those same chains appear to be cross-linked in the small unit cell.

High-temperature phase structure (360 K)

Raw data frames were read by the program SAINT and integrated using 3D profiling algorithms. The resulting data were reduced to produce hkl reflections and their intensities and estimated standard deviations. The data were corrected for Lorentz and polarization effects and numerical absorption corrections were applied based on indexed and measured faces.

The structure was solved and refined in *SHELXTL2014*, using full-matrix least-squares refinement. The non-H atoms were refined with anisotropic thermal parameters and all of the H atoms were calculated in idealized positions and refined riding on their parent atoms. Unit cell determinations attempts were carried out at 320 K and 330 K but were not satisfactory. Data sets of a crystal were then collected at 350 and 360K and resulted in the tetragonal unit cell as the most acceptable. The data however was of low quality as can be evidenced by the poor shape of the diffraction spots. Structure solutions from both data sets could only reveal the $CuCl_4^{-2}$ ions to be ordered. The atoms of the amino alkyl cations could not be located as the Difference Fourier maps revealed a jumble of scattered electron density. An ideal chain of N-C6 was used along with FRAG/FEND to orient it in the most acceptable fit with the electron density maps. After which, atoms were picked up from successive Difference Fourier maps and as they did not refine properly, they were constrained to maintain a similar geometry to the first N-C6 idealized group. Finally, the rest of the possible groups were identified and constrained in a similar fashion. We included two parts for each location of these groups. The $CuCl_4^{-2}$ were treated anisotropically but all other partial atoms were refined isotropically (using EADP command in SHELXL2014) with their displacement parameters make to remain equivalent during the refinement. In the final cycle of refinement of the high temperature phase, 2396 reflections (of which 1590 are observed with $I > 2\sigma(I)$) were used to refine 93 parameters and the resulting R_1, wR_2 and S (goodness of fit) were 11.80%, 28.76% and 2.180, respectively. The refinement was carried out by minimizing the wR_2 function using F^2 rather than F values. R_1 is calculated to provide a reference to the conventional R value but its function is not minimized.

Table S2. Selected structural parameters of C6CuCl obtained by single-crystal X-ray diffraction below and above the phase transition, T_t = 308 K[a]

C6CuCl	**$T < T_t$ (233 K)**	**$T > T_t$ (360 K)**
Space group	P-1	I-4
a	10.4935(4)	7.4676(12)
b	10.5081(4)	7.4676(12)
c	18.6574(7)	39.5644(95)
V	2002.43(13)	2206.31(89)
M–M distance	5.2351(2)	5.2804(6)
M–Cl distance ⊥ c	2.2875(12), 2.9830(11)	2.2887(3), 2.9940(3)
M–Cl distance // c	2.2944(18), 2.2937(17)	2.2647(5), 2.2706(5)
M–Cl–M angle	166.604(49)	176.628(5)
Cl–M–Cl angle	86.913(35), 89.567(53), 93.750(35)	88.054(6), 91.427(5), 91.946(6)

[a]distances are expressed in Ångstroms, and angles are expressed in degrees.

S3) PXRD Patters of LTP and HTP of C6CuCl

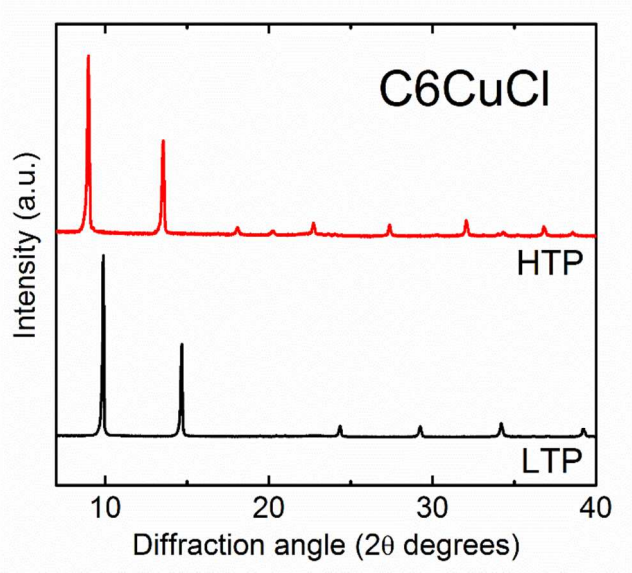

Figure S1. PRXD patterns for the LTP (black line, collected at 298 K) and HTP (red curve, collected at 320 ± 5 K) of the C6CuCl hybrid perovskite. Note the crystalline sample has a highly preferred (c axis) orientation. The interlayer distances calculated from the patterns correspond to 18.29 ± 0.11 Å and 19.57 ± 0.07 Å for the LTP and HTP, respectively. The structural change is reversible, and the HTP returns to the LTP as soon as the temperature drops below the phase transition temperature T_t = 308 K.

S4) AFM Image and Section Analysis of the C6CuCl Nanosheets

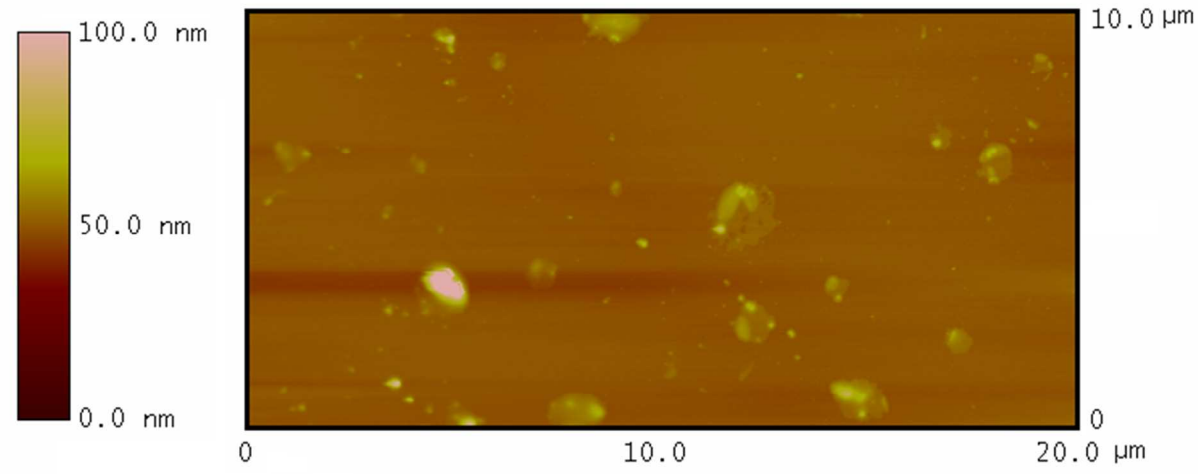

Figure S2. Atomic force microscopy image of the copper chloride perovskite nanosheets after dispersion in toluene and dropped on a clean silicon substrate.

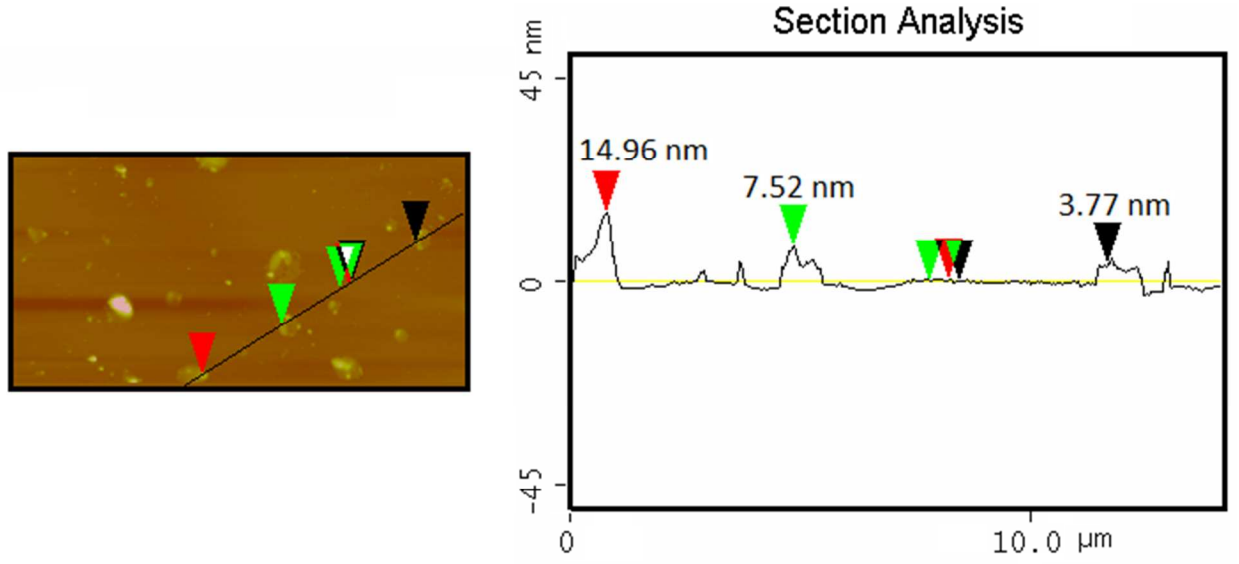

Figure S3. Section analysis of the C6CuCl nanosheets on a silicon substrate showing platelets of thickness under 15 nm.

S5) SEM Images of Thick C6CuCl Platelets

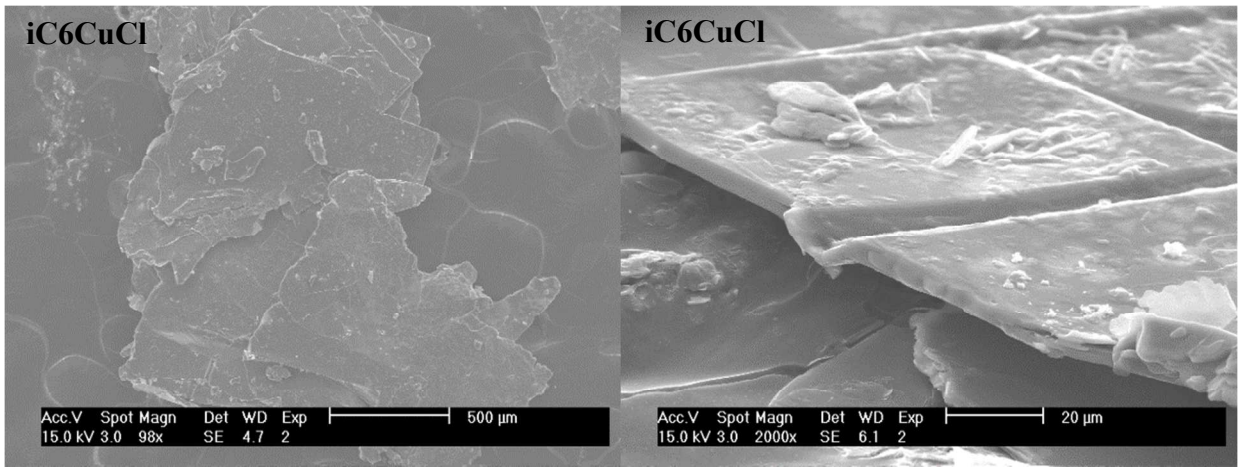

Figure S4. SEM images of 3 µm thick hexylammonium copper(II) chloride platelets, labeled as iC6CuCl.

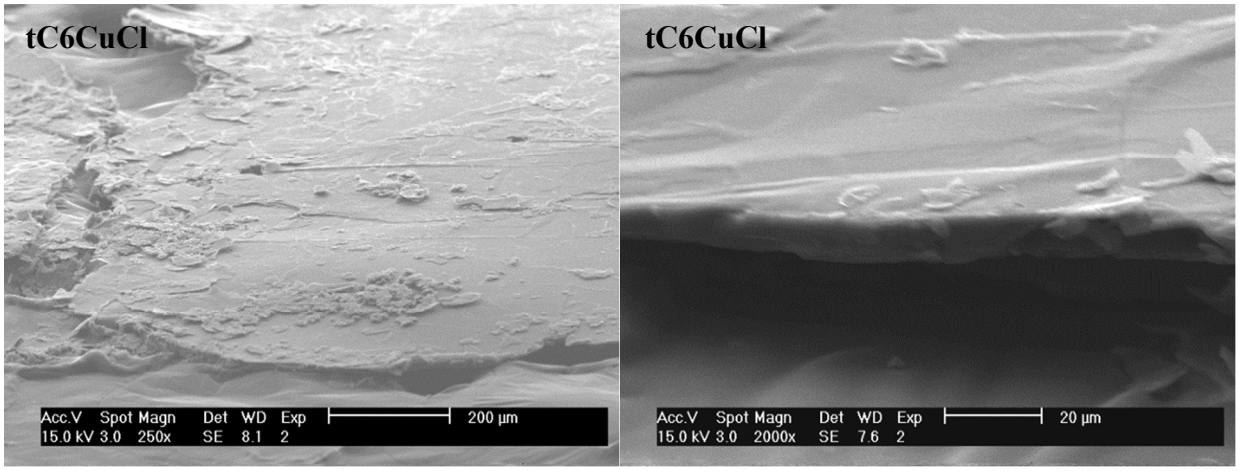

Figure S5. SEM micrographs of the 7 µm thick hexylammonium copper(II) chloride perovskite particles, abbreviated as tC6CuCl.

S6) PXRD of the iC6CuCl and tC6CuCl Dry and in Toluene

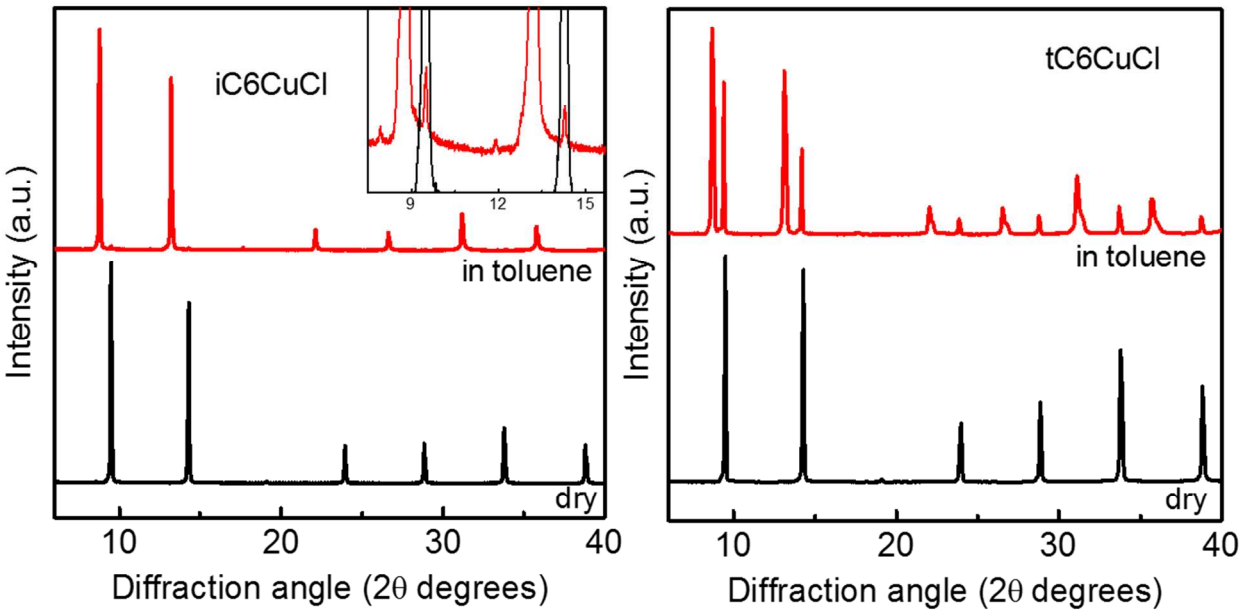

Figure S6. PXRD patterns for the intermediate thickness (iC6CuCl, left) and the thick (tC6CuCl, right) platelets for the copper chloride perovskite analogue. The black solid lines represent the material in its dry state, whereas the red lines show the PXRD pattern of the compound in liquid toluene. The structural phase transitions observed are exactly the same as the ones observed for the polycrystalline powder. The plot on the left for the iC6CuCl illustrates an almost complete phase transition, with the inset showing the presence of the LTP for the (004) and (006) reflections. Whereas the incomplete phase transition is clearly observed for the tC6CuCl in the graph on the right.

S7) PXRD Patters of Toluene-drying C6CuCl Perovskite

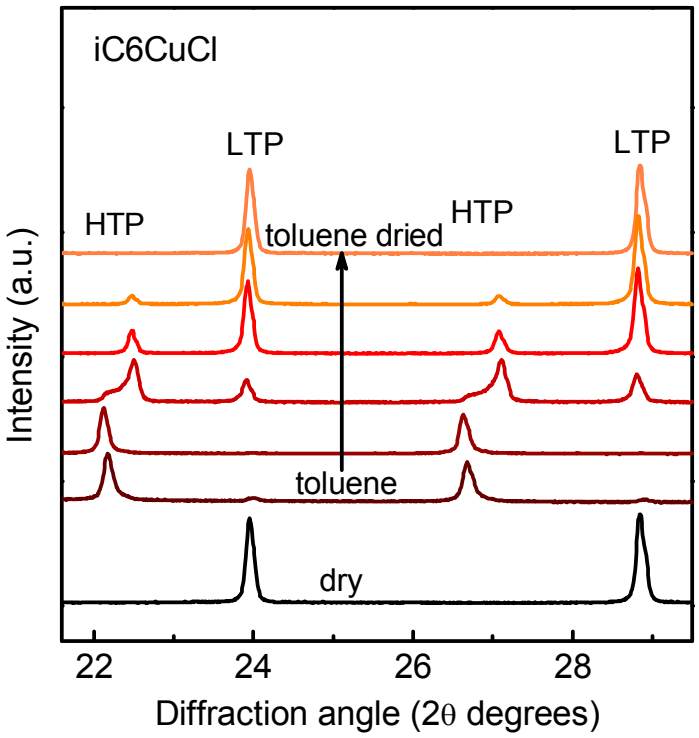

Figure S7. (0010) and (0012) reflections of the PXRD patterns of the C6CuCl perovskite in its dry state (black) and as liquid toluene evaporates (different shades of red). A large structural transformation occurs after wetting with toluene. As the solvent evaporates, the HTP is observed to continuously shift to higher 2θ angles. The material returns to its original LTP after toluene is completely gone.

S8) DSC Plots for Decylammonium Cadmium(II) Chloride

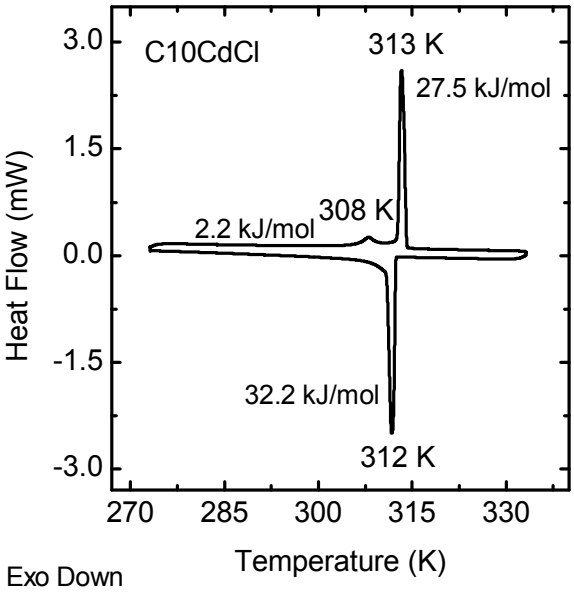

Figure S8. DSC diagram of the decylammonium cadmium(II) chloride, abbreviated as C10CdCl, in the dry state, showing a major solid-solid structural phase transition at around 313 K.

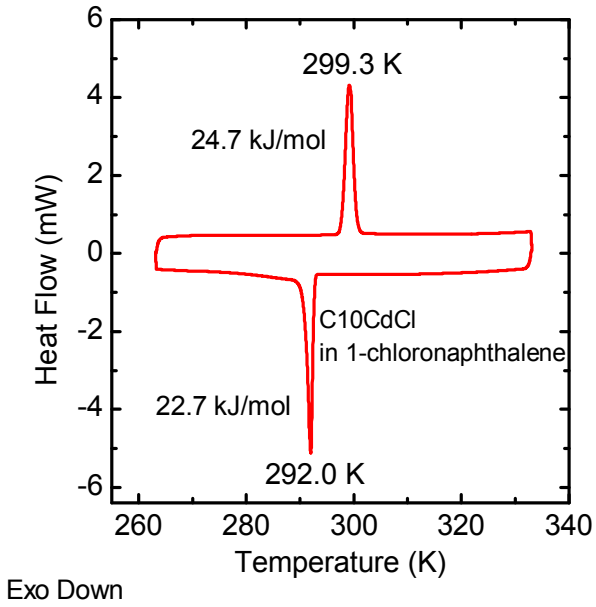

Figure S9. DSC plot of the C10CdCl halide perovskite suspended in 1-chloronaphthalene. Similar to the other 2D halide perovskites investigated in this work, the decylammonium cadmium(II) chloride material also experiences a shift of its solid state phase transition to lower temperatures upon wetting with organic solvent.

S9) PXRD Patterns for Decylammonium Cadmium(II) Chloride

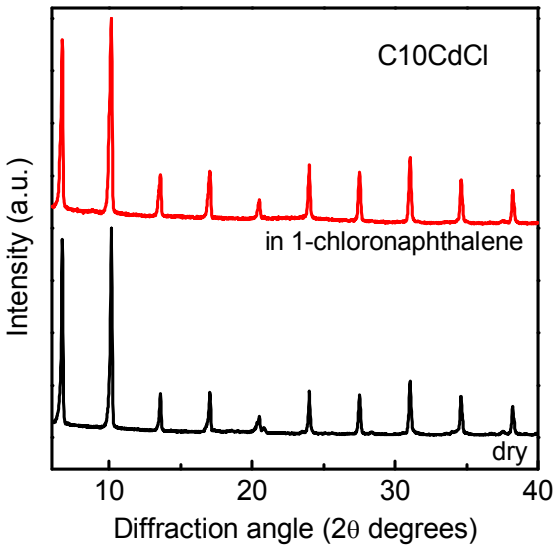

Figure S10. PXRD patterns of sample C10CdCl collected under ambient conditions at 298 K for the material dry (black line) and wet with liquid 1-chloronaphthalene (red line).

S10) VT-PXRD Patterns of the C10CdCl in the Dry State and in 1-chloronaphthalene

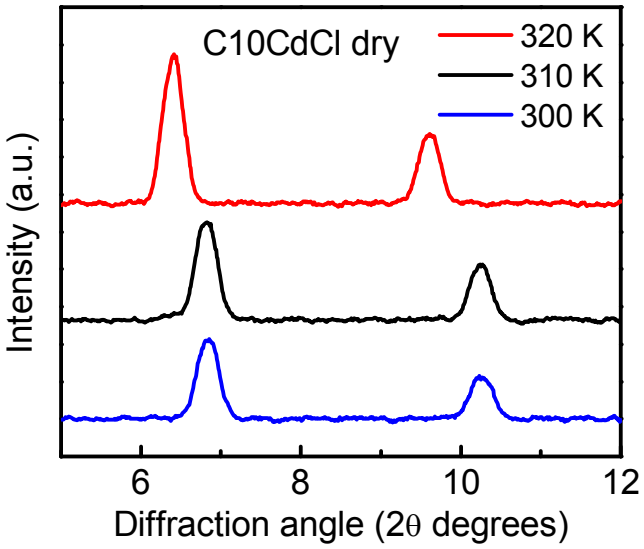

Figure S11. VT-PXRD patters of the C10CdCl perovskite analogue in the dry state showing the (004) and (006) reflections. Data were collected upon warming of the sample at three different temperatures: below the structural phase transition at 300 K (blue); right before the transition at 310 K (black); and above the solid-state phase transition at 320 K (red). An expansion of the interlayer spacing from 25.8 Å to 27.5 Å is observed upon heating the material above the phase transition.

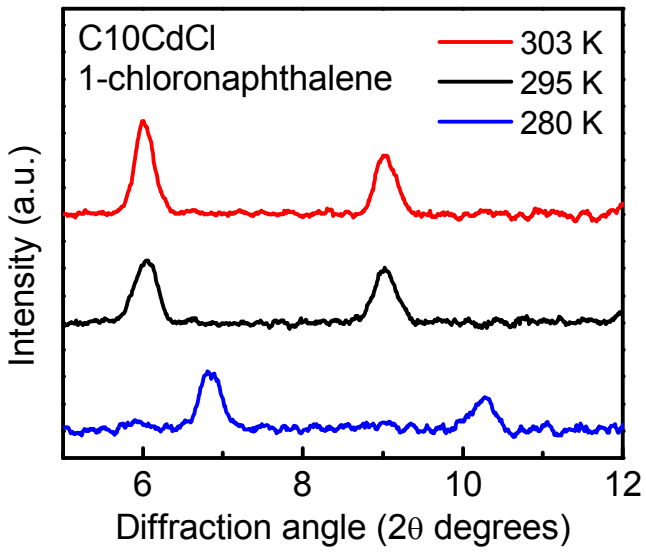

Figure S12. VT-PXRD patterns of the C10CdCl halide perovskite immersed in 1-chloronaphthalene displaying the (004) and (006) reflections. Data were collected upon cooling of the system at three different temperatures: above the phase transition at 303 K (red); right above the transition at 295 K (black); and below the structural phase transition at 280 K (blue). When above the phase transition temperature and immersed in 1-chloronaphthalene the compound exhibits a significantly expanded interlayer distance of 29.4 Å. Upon cooling of the system below the phase transition, the interlayer spacing of the C10CdCl analogue in 1-chloronaphthalene contracts to its LTP distance of 25.8 Å, strongly suggesting intercalation of solvent molecules into the halide perovskite structure does not occur.

S11) DSC Diagrams for C6CdCl

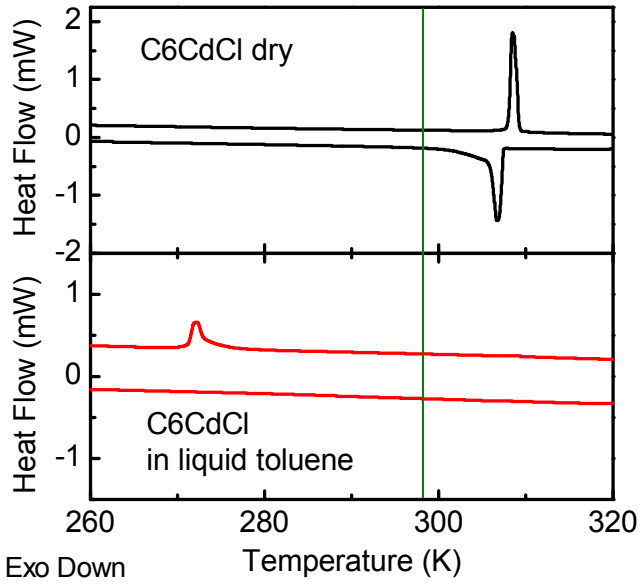

Figure S13. DSC diagram of the C6CdCl perovskite in the dry state (black solid line, top) and suspended in liquid toluene (red line, bottom). The solid state phase transition temperature shifts from above to below room temperature upon suspending the material in liquid toluene.

S12) PXRD Patterns for C6CdCl

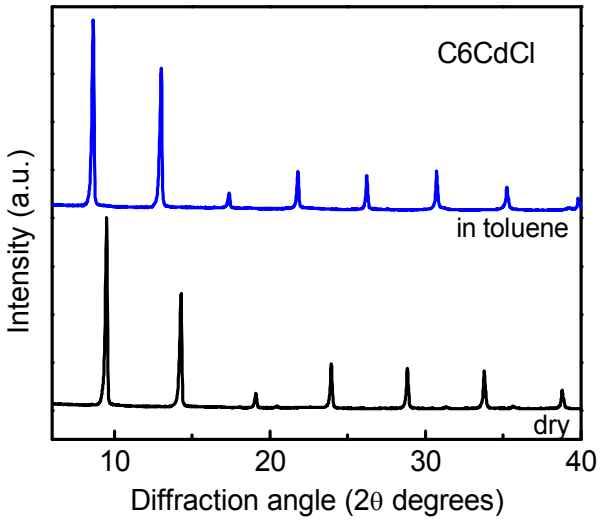

Figure S14. PXRD patterns collected at ambient conditions for the C6CdCl hybrid perovskite in the dry state (black line), and wet with liquid toluene (blue line). The shift of the (002l) reflection to lower 2θ angles upon wetting of the powder with toluene is clearly observed and indicates an expansion of the interlayer spacing of the perovskite, very similar to the behavior of the hexylammonium copper(II) chloride analogue discussed in the main paper.